Published in final edited form as:
Pain. 2008 July 31; 137(3): 507–519. doi:10.1016/j.pain.2007.10.013.

TNF signaling contributes to the development of nociceptive sensitization in a tibia fracture model of complex regional pain syndrome type I

Ilya Sabsovich[a,b], **Tian-Zhi Guo**[a], **Tzuping Wei**[a], **Rong Zhao**[a], **Xiangqi Li**[b], **David J. Clark**[b], **Christian Geis**[c], **Claudia Sommer**[c], and **Wade S. Kingery**[a,d*]

a*Physical Medicine and Rehabilitation Service, Veterans Affairs Palo Alto Health Care System, Palo Alto, CA*

b*Anesthesiology Service, Veterans Affairs Palo Alto Health Care System Palo Alto, CA, and Department of Anesthesia, Stanford University School of Medicine, Stanford, CA*

c*Department of Neurology, Julius-Maximilians-Universitat, Wurzburg, Germany*

d*Department of Orthopedic Surgery, Stanford University School of Medicine, Stanford, CA*

Abstract

Tibia fracture in rats initiates a cascade of nociceptive, vascular, and bone changes resembling complex regional pain syndrome type I (CRPS I). Previous studies suggest that the pathogenesis of these changes is attributable to an exaggerated regional inflammatory response to injury. We postulated that the pro-inflammatory cytokine tumor necrosis factor alpha (TNF) might mediate the development of CRPS-like changes after fracture. RT-PCR and EIA assays were used to evaluate changes in TNF expression and content in skin, nerve, and bone after fracture. Bilateral hindpaw thickness, temperature, and nociceptive thresholds were determined, and bone microarchitecture was measured using microcomputed tomography. Lumbar spinal cord Fos immunostaining was performed for quantification of Fos positive neurons. After baseline testing the distal tibia was fractured and the hindlimb casted for 4 weeks. The rats were subcutaneously injected either with a soluble TNF receptor type 1 (sTNF-R1, 5mg/kg/d) or saline every 3 days over 28 days and then were retested at 4-weeks post-fracture. Tibia fracture chronically upregulated TNF expression and protein levels in the hindpaw skin and sciatic nerve. After fracture the rats developed hindpaw mechanical allodynia and unweighting, which were reversed by sTNF-R1 treatment. Consistent with the behavioral data, spinal Fos increased after fracture and this effect was inhibited by sTNF-R1 treatment. Collectively, these data suggest that facilitated TNF signaling in the hindlimb is an important mediator of chronic regional nociceptive sensitization after fracture, but does not contribute to the hindlimb warmth, edema, and bone loss observed in this CRPS I model.

Correspondence should be addressed to Wade S. Kingery, M.D., Physical Medicine and Rehabilitation Service (117), Veterans Affairs Palo Alto Health Care System, 3801 Miranda Ave., Palo Alto, CA 94304, Tel: 650-493-5000 ext 64768, Fax: 650-852-3470, E-mail: wkingery@stanford.edu.

Keywords

tibia fracture; neuropathic pain; TNF; sTNF-R1; microCT scanning; Fos immunoreactivity; complex regional pain syndrome

1. Introduction

Previously proposed complex regional pain syndrome (CRPS) animal models have not reproduced the inciting trauma and the nociceptive, vascular and bone changes observed in the CRPS patient. CRPS type I is a frequent sequelae of distal tibia (Sarangi et al. 1993) and radius fractures (Atkins et al. 1990). The affected limb presents with an initial increase in skin temperature (Birklein et al. 1998), increased cutaneous protein extravasation (Oyen et al. 1993), distal limb edema (Veldman et al. 1993), pain, and allodynia (Blumberg and Janig 1994). Periarticular osteoporosis also develops in the fracture limb (Bickerstaff et al. 1993; Sarangi et al. 1993). Recently we described a rat fracture model that closely resembles the clinical scenario (Guo et al. 2004). After distal tibia fracture rats develop chronic unilateral hindlimb warmth, edema, facilitated spontaneous protein extravasation, allodynia, unweighting, and periarticular osteoporosis, changes resembling those observed in CRPS I patients.

We postulate that the enhanced vascular permeability, edema, warmth, redness, and vasodilatation observed in CRPS could be attributable to an enhanced neurogenic inflammatory response mediated by substance P (SP). Peripherally released SP is able to elicit vasodilatation and protein extravasation via activation of the neurokinin 1 (NK1) receptor (McDonald 1988; Bowden et al. 1994). The same mechanism facilitates sensitization of second-order spinal neurons via activation of the NK1 receptors on ascending spinal neurons, resulting in spontaneous pain and hyperalgesia (Benoliel et al. 1999; Nichols et al. 1999). NK1 antagonists partially reverse the warmth, edema, spontaneous extravasation, and allodynia observed after tibia fracture (Guo et al. 2004), evidence that SP signaling contributes to the vascular and nociceptive sequelae of fracture.

SP also stimulates the production of the pro-inflammatory cytokines in the skin and leukocytes of rats (Dickerson et al. 1998; Saade et al. 2002; Delgado et al. 2003). TNF is at the top of the cytokine pro-inflammatory cascade and TNF inhibitors have proven to be selective and highly effective therapeutics for rheumatoid arthritis and a variety of chronic inflammatory diseases (Feldmann 2002). There is also evidence of increased inflammatory cytokine expression in the skin of CRPS patients and anecdotal evidence that TNF inhibitors reduce spontaneous and articular pain in CRPS patients (Huygen et al. 2002; Huygen et al. 2004a). Furthermore, increased serum levels of sTNF-R1 have been positively correlated to the presence of mechanical allodynia in polyneuropathy (Empl et al. 2001) and CRPS (Maihofner et al. 2005) patients.

Collectively, these data suggest that trauma induced facilitated SP signaling could stimulate TNF over-expression in an injured limb, resulting in periarticular bone loss, joint tenderness and the development of chronic pain. The objectives of the current study were to map post-fracture changes in cytokine TNF expression and content in skin, nerve, and bone and evaluate the effects of a TNF antagonist (sTNF-R1) on the development of nociceptive, vascular, and bone changes after fracture.

2. Materials and methods

These experiments were approved by our institute's Subcommittee on Animal Studies and followed the guidelines of the IASP (Zimmermann 1983). Adult (10-month-old) male Sprague

Dawley rats (Harlan, Indianapolis, IN) were used in all experiments. The animals were housed individually in isolator cages with solid floors covered with 3 cm of soft bedding and were fed and watered *ad libitum*. During the experimental period the animals were fed Lab Diet 5012 (PMI Nutrition Institute, Richmond, IN), which contains 1.0% calcium, 0.5% phosphorus, and 3.3 IU/g of vitamin D_3.

2.1 Surgery

Tibia fracture was performed under isoflurane anesthesia as we have previously described (Guo et al. 2004; Guo et al. 2006). The right hindlimb was wrapped in stockinet (2.5 cm wide) and the distal tibia was fractured using pliers with an adjustable stop (Visegrip, Petersen Manufacturing, Dewitt, NE) that had been modified with a 3-point jaw. The hindlimb wrapped in casting tape (Delta-Lite, Johnson & Johnson, Raynham, MA) so the hip, knee and ankle were flexed. The cast extended from the metatarsals of the hindpaw up to a spica formed around the abdomen. The cast over the paw was applied only to the plantar surface; a window was left open over the dorsum of the paw and ankle to prevent constriction when post-fracture edema developed. To prevent the animals from chewing at their casts, the cast material was wrapped in galvanized wire mesh, which was attached by wires inserted into holes drilled in the cast. After fracture and casting the rats were given subcutaneous saline and 2 days of buprenorphine (0.3 mg/kg) for post-operative hydration and analgesia. At 4 weeks the rats were anesthetized with isoflurane and the cast removed with a vibrating cast saw. All rats used in this study had union at the fracture site after 4 weeks of casting.

2.2 RNA isolation and Real-Time PCR

The RNA was isolated from hindpaw skin using our previously described methods (Liang et al. 2003). Briefly, under isoflurane anesthesia the hindpaw skin was collected by dissection and disrupted rapidly in a Dounce homogenizer. Total RNA was then isolated using purification columns as directed (RNeasy reagents; Qiagen, Valencia, CA). Before RNA purification samples were first homogenized using a Polytron device (Brinkman Instruments Inc., Westbury, NY), then centrifuged for 10 min at 12,000g at 4C. The supernatants were processed using the RNeasy Mini Kit (Qiagen) according to manufacturer's instructions. The purity and concentration of the purified RNA was determined spectrophotometrically. cDNA was subsequently prepared from 1 μg RNA in a 25 μl final volume using random hexamer primers and Superscript reverse transcriptase according to the accompanying protocol (Invitrogen, Carlsbad, CA). The cDNA reactions were diluted 1:8 in nuclease-free water before further analysis.

Real-time quantitative PCR (qPCR) was carried out using the SYBR® green reporter dye and protocol (Applied Biosystems; Foster City, CA). Briefly, 2 μl of a mixture of 2x SYBR green and TNF primers (forward primer: AAATGGGCTCCCTCTCATCAGTTC; reverse primer: TCTGCTTGGTGGTTTGCTACGAC) were loaded with 2 μl diluted cDNA template in each well. Eight μl mineral oil was then loaded in each well to prevent loss of solution. Thermal cycling utilized an Applied Biosystems 7900HT system with a 5-min denaturation step at 95° C followed by 40 cycles of 95°C 30 sec/60°C 30 sec/72°C 60 sec). Melting curves were performed to document single product formation, agarose electrophoresis confirmed product size, and restriction enzyme digestion confirmed product identity. The amplification of 18S RNA was used as an internal control. The 18S primers were purchased from Ambion (18S forward primer: AGGAATTGACGGAAGGGCAC; 18S reverse primer: GTGCAGCCCCGGACATCTAAG, Austin, TX, USA). Amplification kinetics for the two amplification products was found to be similar. The data from real-time PCR experiments were analyzed by the comparative CT method as described in the manual for the ABI prism 7900 real-time system. Briefly, the parameter C_t was derived for each cDNA sample and primer pair; C_t is an expression of amplification kinetics referring to the cycle at which log-phase

amplification reaches a pre-determined threshold. For a given sample, C_t values for 18S RNA were subtracted from the C_t of TNF to arrive at a ΔC_t value. The mean ΔC_t from all control animal reactions was then subtracted from the mean ΔC_t for the treated samples to arrive at $\Delta\Delta C_t$. This parameter reflects the fold difference of over- or underexpression of TNF in fracture rat ipsilateral hindpaw skin tissue relative to control according to the expression $2^{-\Delta\Delta Ct}$. In each experiment samples were analyzed in triplicate or quadruplicate for the indicated numbers of rats.

To confirm the specificity of amplified product the dissociation curves for PCR reaction products were analyzed. Only one peak was observed for TNF mRNA and the amplification kinetics for 18S and TNF were quite similar (data not shown). Ethidium bromide staining of PCR products on conventional agarose gels demonstrated product bands of the expected sizes (Fig.1B).

2.3 Homogenization procedure and ELISA

Rat sciatic nerve, hind paw dorsal skin and proximal tibia were collected at 4 weeks after fracture and frozen immediately on dry ice. All tissues were cut into fine pieces in ice-cold phosphate buffered saline (PBS), pH 7.4, containing protease inhibitors (aprotinin (2 μg/ml), leupeptin (5 μg/ml), pepstatin (0.7 μg/ml), and PMSF (100 μg/ml); Boehringer Mannheim, Germany) followed by homogenization using a rotor/stator homogenizer. Homogenates were centrifuged for 5 min at 14 000g at 4°C. Supernatants were transferred to fresh precooled Eppendorf tubes. Triton X-100 (Boehringer Mannheim, Germany) was added at a final concentration 0.01 %. The samples were centrifuged again for 5 min at 14 000g at 4°C. The supernatants were aliquoted, stored at −80°C and assayed in duplicate (after dilution in the standard buffer supplied) by a rat TNF Elisa kit (Biosource Europe, Nivelle, Belgium) according to the manufacturer's instructions. This assay system detects rat TNF with a sensitivity of 4 pg/ml. Positive and negative controls were included in each assay. TNF concentration was expressed as pg/mg protein. Protein content was determined by the bicinchoninic acid protein assay reagent (Pierce, KMF Laborchemie, St. Augustin, Germany).

2.4 Drugs

Soluble tumor necrosis factor receptor type 1 (sTNF-R1) conjugated with polyethylene glycol (PEG) was produced at Amgen (Thousand Oaks, CA, USA). sTNF-R1 is a recombinant *E. coli* form of the human 'high-affinity' p55 tumor necrosis factor receptor (TNFR1) to which a 30 kd PEG molecule is attached (Edwards et al. 1998; Grell et al. 1998; Martin et al. 1998). The effects of the TNF alpha and TNF beta (also known as lymphotoxin alpha) cytokines are mediated through binding to the p55 (TNFR1) and p75 (TNFR2) cell surface TNF receptors and sTNF-R1 selectively binds to both of these cytokines with high affinity (personal communication, Amgen). Fracture rats were subcutaneously injected with sTNF-R1, which acts as a soluble decoy receptor for TNF that competitively inhibits TNF binding to cell surface TNF receptors, thus acting as a selective TNF antagonist. The dosage and administration protocol for sTNF-R1 (5mg/kg given subcutaneously every third day) was based on previous studies using sTNF-R1 treatment in arthritic rats (Bendele et al. 1999a; Bendele et al. 1999b; McComb et al. 1999; Feige et al. 2000).

2.5 Hindpaw nociception

To measure mechanical allodynia in the rats an up-down von Frey testing paradigm was used as we have previously described (Kingery et al. 2003). Rats were placed in a clear plastic cylinder (20 cm in diameter) with a wire mesh bottom and allowed to acclimate for 15 minutes. The paw was tested with 1 of a series of 8 von Frey hairs ranging in stiffness from 0.41 g to 15.14 g. The von Frey hair was applied against the hindpaw plantar skin at approximately midsole, taking care to avoid the tori pads. The fiber was pushed until it slightly bowed and

then it was jiggled in that position for 6 seconds. Stimuli were presented at an interval of several seconds. Hindpaw withdrawal from the fiber was considered a positive response. The initial fiber presentation was 2.1 g and the fibers were presented according to the up-down method of Dixon to generate 6 responses in the immediate vicinity of the 50% threshold.

An incapacitance device (IITC Inc. Life Science. Woodland, CA) was used to measure hindpaw unweighting. The rats were manually held in a vertical position over the apparatus with the hindpaws resting on separate metal scale plates and the entire weight of the rat was supported on the hindpaws. The duration of each measurement was 6 seconds and 10 consecutive measurements were taken at 60-second intervals. Eight readings (deducting the highest and lowest ones) were averaged to calculate the bilateral hindpaw weight bearing values.

2.6 Hindpaw volume

A laser sensor technique was used to determine the dorsal-ventral thickness of the hindpaw, as we have previously described (Kingery et al. 2003). Before baseline testing the bilateral hindpaws were tattooed with a 2–3 mm spot on the dorsal skin over the midpoint of the third metatarsal. For laser measurements each rat was briefly anesthetized with isoflurane and then held vertically so the hindpaw rested on a table top below the laser. The paw was gently held flat on the table with a small metal rod applied to the top of the ankle joint. Using optical triangulation, a laser with a distance measuring sensor was used to determine the distance to the table top and to the top of the hindpaw at the tattoo site and the difference was used to calculate the dorsal-ventral paw thickness. The measurement sensor device used in these experiments (4381 Precicura, Limab, Goteborg, Sweden) has a measurement range of 200 mm with a 0.01 mm resolution.

2.7 Hindpaw temperature

The room temperature was maintained at 23°C and humidity ranged between 25–45%. The temperature of the hindpaw was measured using a fine wire thermocouple (Omega, Stanford, CT) applied to the paw skin, as previously described (Kingery et al. 2003). The investigator held the thermistor wire using an insulating Styrofoam block. Three sites were tested over the dorsum of the hindpaw; the space between the first and second metatarsals (medial), the second and third metatarsals (central), and the fourth and fifth metatarsals (lateral). After a site was tested in one hindpaw the same site was immediately tested in the contralateral hindpaw. The testing protocol was medial dorsum right then left, central dorsum right then left, lateral dorsum right then left, medial dorsum left then right, central dorsum left then right, and lateral dorsum left then right. The six measurements for each hindpaw were averaged for the mean temperature.

2.8 Fos spinal cord immunohistochemistry

Rats were euthanized with CO_2 and perfused intracardially with 200 ml 0.1 M PBS followed by 200 ml neutral 10% buffered formaldehyde. Spinal cord segments (L3–L5) were removed, post-fixed in the perfusion fixative overnight and cryoprotected in 30% sucrose at 4°C for 24 h. Serial frozen spinal cord sections, 40-mm-thick, were cut on a coronal plane by using a sliding microtome, collected in PBS, and processed as free floating sections. Fos immunostaining was performed as previously described (Sawamura et al. 2000). Because the sciatic nerve projects heavily to the L3–L5 segments of the spinal cord, we analyzed the numbers of Fos immunoreactive (Fos-IR) neurons at that level.

To evaluate and compare the distribution of Fos positive neurons in the lumbar spinal cord, a Bioquant image analysis system (Bioquant, Nashville, TN) attached to Nikon Eclipse 80i microscope was used. Images were captured using 10X magnification, converted to digital and Fos-IR neurons were identified by dense black staining of the nucleus. The Fos-IR neurons

were plotted and counted with Bioquant Automated Imaging module through four arbitrary defined regions of the spinal grey matter of the L3 – L5 segments, according to the cytoarchitectonic organization of the spinal cord (Rexed 1952; Molander and Grant 1986); the superficial laminae (laminae I – II), the nucleus proprius (laminae III – IV), and the deep laminae (laminae V – VI; neck) of dorsal horn, and the ventral horn (laminae VII – X). For each section, the Fos-IR neurons were counted for each lamina, the counts were pooled, and the average number was calculated giving a count that was the mean of all stained neurons in those three sections per each cytoarchitectonic region. The investigator responsible for plotting and counting of the Fos-IR neurons was unaware of the origin of the sections.

2.9 Microcomputed tomography (μCT)

Ex vivo scanning was performed for assessment of trabecular and cortical bone architecture using μCT (VivaCT 40, Scanco Medical AG, Basserdorf Switzerland). Specifically, trabecular bone architecture was evaluated at the distal femur and fourth lumbar vertebra and cortical bone morphology was evaluated at the femur midshaft. CT images were reconstructed in 1024 × 1024-pixel matrices for vertebral, distal femur, and midfemur samples and stored in 3-D arrays. The resulting grayscale images were segmented using a constrained Gaussian filter to remove noise, and a fixed threshold (25.5% of the maximal grayscale value for vertebrae, 25.5% for distal femur and 35% for midfemur cortical bone) was used to extract the structure of the mineralized tissue. The μCT parameters set at threshold = 255, $\sigma = 0.8$, support = 1 for vertebral samples, threshold = 255, $\sigma = 0.8$, support = 1 for distal femur, and threshold = 350, $\sigma = 1.2$, and support = 2 for midfemur evaluation analysis. A single operator outlined the trabecular bone region within distal femur and vertebral body, and cortical bone region in midfemur shaft.

All spinous processes were removed for L_4 vertebrae scanning and 8 samples were fixed in a notched plexiglas holder for batch scanning. Each vertebral body was scanned using 223 transversely oriented 21μm thick slices (21-μm isotropic voxel size) encompassing a length of 4.68mm. The trabecular bone region was manually identified and all slices containing trabecular bone between the growth plates were included for analysis. In the distal femur 150 transverse slices of 21μm thickness (21-μm isotropic voxel size) encompassing a length of 3.15mm were acquired, but only 100 slices encompassing 2.1mm of the distal femur were evaluated, starting where the growth plate bridge across the middle of the metaphysis ends. The region of interest (ROI) was manually outlined on each CT slice, extending proximally from the growth plate. At the femur midshaft, 10 transverse CT slices were obtained, each 21 μm thick totaling 0.21 mm in length (21 μm isotropic voxel size) and these were used to compute the cortical bone area (BAr, mm^2) and other cortical bone parameters.

The vertebral and distal femur trabecular bone basic structural parameters, including bone volume fraction (BV/TV, %), trabecular number (Tb.N, mm^{-1}), trabecular thickness (Tb.Th, μm), trabecular separation (Tb.Sp,μm), structure model index (SMI), and connectivity density (Conn.D, mm^{-3}) were measured in three dimensions using direct 3D morphometry based on the distance transformation (Hildebrand and Ruegsegger 1997a; Hildebrand et al. 1999), without assumptions regarding the underlying bone architecture (Hildebrand and Ruegsegger 1997b; 1997a). The connectivity of a two-component system, i.e., bone and marrow, was defined directly as if all trabecular and bone marrow cavities are connected without isolated marrow cavities inside the bone (Mashiba et al. 2001). It was normalized by examined tissue volume and reported as Conn.D.

2.10 Study design

Baseline determinations were made of bilateral hindpaw temperature, thickness, mechanical nociceptive withdrawal thresholds, and weighting bearing. After baseline tests the rats

underwent a right distal tibia fracture with casting. The casts were removed after 28 days and repeat bilateral testing of hindpaw temperature, thickness, mechanical nociceptive withdrawal thresholds, and weighting bearing was performed. The rats were subcutaneously injected either with sTNF-R1 (200μl, 5mg/kg/d) or saline every third day, starting the day before the fracture, over the 28 day post-fracture interval. Hindpaw temperature, thickness, and mechanical nociceptive thresholds data were analyzed as the difference between the treatment side and the contralateral untreated side. Right hindpaw weight bearing data was analyzed as a ratio between the right hindpaw weight and the sum of right and left hindpaws values ((2R/(R+L)) × 100%). *Ex vivo* μCT scanning was used to determine vertebral and femoral bone parameters for control rats (no fracture) and fracture rats that were subcutaneously injected with either sTNF-R1 or saline. Spinal cord Fos protein expression was determined at 4 weeks after right tibia fracture. There were three treatment groups: control rats (no fracture) and fracture rats that were subcutaneously injected with either sTNF-R1 or saline for 4 weeks, starting a day before the tibia fracture.

2.11 Statistical analysis

Statistical analysis was accomplished using a one-way analysis of variance (ANOVA) followed by *post hoc* Newman-Keuls multiple comparison testing to compare between the control cohort and the fracture rat cohorts that were injected with either sTNF-R1 or saline. Pearson correlation analysis was performed to determine associations between behavioral tests and Fos expression. All data are presented as the mean ± SE of the mean, and differences are considered significant at a p value less than 0.05 (Prism 4, GraphPad Software, San Diego, CA).

3. Results

3.1 Increased expression of TNF mRNA in hindpaw skin following distal tibia fracture in rats

Four weeks after fracture (n = 14) the TNF mRNA levels in the ipsilateral hindpaw skin were 7.5-fold greater than mRNA levels from control rats (n = 10, Fig. 1A). Contralateral hindpaw skin TNF mRNA did not significantly differ from controls (Fig. 1A).

3.2 Increased expression of TNF protein in skin and nerve tissue of fracture rats

TNF protein levels were determined by ELISA in hindpaw skin (Fig. 2A), proximal tibia trabecular bone (Fig. 2B), and sciatic nerve (Fig. 2C) at 4 weeks post-fracture. After fracture (n = 14) TNF levels were higher in the ipsilateral hindpaw skin and sciatic nerve relative to controls (n = 7). TNF levels were also higher in the contralateral hindpaw skin after fracture vs controls. but there was no significant change in TNF levels in the ipsilateral tibia trabecular bone vs control. After fracture the TNF levels in the ipsilateral limb were consistently higher than TNF levels in the contralateral limb in all 3 tissues.

3.3 sTNF-R1 effect on hindpaw vascular and nociceptive parameters after distal tibia fracture

The effects of sTNF-R1 treatment on fracture induced hindpaw warmth, edema, mechanical sensitivity and weight bearing were evaluated (Fig.3). Rats were injected with either sTNF-R1 (5mg/kg/d every third day, n = 8) or saline (n = 7) subcutaneously for four weeks after the fracture. At 4 weeks post-fracture the right hindpaw thickness (Fig. 3A) and temperature (Fig. 3B) were increased in the saline injected fracture rats compared to controls, and sTNF-R1 treatment had no effect on these vascular changes. Figure 3C illustrates that von Frey nociceptive thresholds in the right hindpaw were reduced after fracture, but sTNF-R1 treatment blocked the development of this mechanical allodynia. There was no significant difference between the contralateral hindpaw von Frey withdrawal thresholds in the fracture cohorts or the controls, indicating that the saline treated fracture rats did not develop mechanical allodynia in the contralateral hindpaw and that sTNF-R1 treatment had no effect on mechanical

nociceptive thresholds in the contralateral hindpaw after fracture. Figure 3D illustrates that saline treated fracture rats unweighted the ipsilateral hindpaw by 60% at 4 weeks post-fracture and sTNF-R1 treatment partially reversed this fracture induced unweighting to only 30%.

3.4 sTNF-R1 effect on Fos expression in lumbar spinal cord after distal tibia fracture

Four weeks after the fracture we observed an increase in Fos expression in the ipsilateral dorsal horn (Fig. 4) in laminae I–II (122%), in laminae II–IV (164%), and laminae V–VI (130%) of the lumbar spinal cord in saline treated fracture rats compared to controls (Fig. 5A, B, C). Treatment with sTNF-R1 inhibited or completely blocked this increase in Fos-IR neurons in ipsilateral dorsal horn (Fig. 5A, B). In the contralateral dorsal horn of the saline treated fracture rats there was a significant increase in Fos expression only in laminae V–VI (Fig. 5F) and this increase was blocked by sTNF-R1 treatment (Fig. 5D, E, F).

A Pearson correlation analysis for Fos neuron counts and the mechanical allodynia data was performed. This analysis included results from the control, saline treated fracture, and sTNF-R1 treated fracture rats (n = 12). Correlation analysis identified a strong association between reduced mechanical withdrawal thresholds in the hindpaw and increased numbers of Fos positive neurons in the ipsilateral laminae I–II (Fig. 6A, $p = 0.002$, $R^2 = 0.627$), III–IV (Fig. 6B, $p = 0.002$, $R^2 = 0.627$), and V–VI (Fig. 6C, $p = 0.007$, $R^2 = 0.532$). Thus rats with the greatest mechanical sensitivity tended to have the highest Fos expression in the ipsilateral dorsal horn, indicating that immediate-early gene activation in the spinal cord is a marker for nociceptive sensitization.

3.5 sTNF-R1 had no effect on trabecular and cortical bone loss after fracture

Figure 7 shows μCT scans from control, saline treated fracture, and sTNF-R1 treated fracture rats, demonstrating fracture induced trabecular bone loss in the distal femur and L_4 vertebrae. Treatment with sTNF-R1 had no effect on this post-traumatic regional osteopenia. Table 1 and Figure 8 show quantitative data for the effect of fracture and sTNF-R1 treatment on the distal femur and L_4 vertebral trabecular bone architecture. Fracture reduced BV/TV by 32% in the ipsilateral distal femur ($p < 0.001$) and by 19% in the L_4 vertebra ($p < 0.05$) (panels 8A and 8C respectively). The BV/TV was 13% lower in the distal femur contralateral to the fracture than in controls, but this did not reach significance (panel 8B). Also, Tb.Th was reduced by 9.2% in the ipsilateral distal femur ($p < 0.01$) and by 8.9% in the L_4 vertebra ($p < 0.01$); Conn.D decreased by 37.3% ($p < 0.001$) in the ipsilateral distal femur; and the SMI increased by 25% ($p < 0.001$) and by 15% ($p < 0.05$) in the ipsi- and contralateral distal femur, respectively, and by 87.5% ($p < 0.01$) in the lumbar (L_4) vertebrae indicating a transformation from plate- to rod-like trabecular morphology. No significant changes were observed in any structural index after administration of TNF-R1 vs saline fracture group (Table 1).

3.6 sTNF-R1 had no effect on body mass after fracture

We observed a body weight loss four weeks after the right distal tibia fracture both in saline and sTNF-R1 rats. At 4 weeks after fracture the saline treated rats (n = 7) had lost 22.1% of their body mass (539 ± 16 g baseline *vs.* 420 ± 14 g at week 4), while sTNF-R1 treated fracture rats (n = 8) had lost 21.3% of their body weight (540 ± 15 g baseline *vs.* 425 ± 20 g at week 4). ANOVA analysis followed by *post hoc* Newman-Keuls multiple comparison testing showed a significant change for both of the fracture groups *vs.* control group (n = 6, $p < 0.001$, data not shown), but there was no difference between sTNF-R1 and saline treatment groups.

Discussion

After distal tibia fracture the rats developed chronic hindlimb edema, warmth, mechanical allodynia, unweighting, increased spinal Fos, and periarticular bone loss, a syndrome closely

resembling CRPS I. Compared to our previous data using the rat tibia fracture model(Guo et al. 2004; Guo et al. 2006), the hindpaw edema (1.21 ± 0.21 mm) and warmth (2.5 ± 0.9 C°) observed in the current study were in the range of our previous results (0.97 ± 0.16 to 2.18 ± 0.46 mm and 1.6 ± 0.7 to 3.9 ± 1.0 C°). Hindpaw mechanical allodynia (−9.7 ± 0.7 g) was greater in the current study than in previous ones (−5.1 ± 0.7 to −6.6 ± 1.8 g), which could be explained by variability of the fracture type, alignment, angulation, callus mechanical properties, or cast tightness, as well as by genetic variability (adult 10-month-old male Sprague Dawley rats were used in all experiments, but we changed vendors from Animal Technologies Limited, Fremont CA to the Harlan, Indianapolis, IN during the course of these studies due to Harlan purchasing and closing Animal Technologies).

The effects of distal tibia fracture were also examined on TNF expression in hindlimb skin, tibia and nerve. Four weeks post-fracture there was an increase in TNF expression in the skin of the fracture hindlimb (Fig. 1), as well as an elevation in TNF protein content in the skin and sciatic nerve in the ipsilateral hindlimb (Fig. 2). As cytokines are normally expressed transiently in response to stimuli, the persistent regional elevation of TNF observed 4 weeks post-fracture indicates ongoing TNF synthesis after fracture, perhaps in response to the chronic post-traumatic neurogenic inflammation that develops in this fracture model (Guo et al. 2004;Guo et al. 2006). Similarly, chronically elevated TNF levels have been observed in skin blister fluid from symptomatic limbs of CRPS type I patients in both the intermediate (6 months post-injury) and chronic (30 months post-injury) phases of the disease (Huygen et al. 2002;Huygen et al. 2004b;Munnikes et al. 2005).

Increased inflammatory cytokine signaling in the skin contributes to the sensory hypersensitivity associated with inflammation. This may be due to the direct activation of cytokine receptors on neurons or indirectly by stimulating the release of agents that act on the neuron. TNF exerts its effects through the TNF receptor 1 (TNFR1) and the TNF receptor 2 (TNFR2) (for review see (Weinberg and Montler 2005)) and studies using TNFR1 (p55) and TNFR2 (p75) knockout mice suggest that the TNFR1 receptor is the primary mediator of TNF nociceptive activity (Cunha et al. 2005; Jin and Gereau 2006; Vogel et al. 2006). Skin nociceptors express TNFR1 receptors and are activated and sensitized by TNF (Sommer and Kress 2004; Myers et al. 2006). Furthermore, the subcutaneous injection of TNF into the rat hindpaw reduces mechanical and heat nociceptive thresholds (Cunha et al. 1992; Woolf et al. 1997; Junger and Sorkin 2000) and these TNF pro-nociceptive effects are lost in TNFR1 knockout mice (Cunha et al. 2005; Jin and Gereau 2006).

Facilitated TNF signaling appears critical for the development of inflammatory pain behavior in several animal models. Blocking TNF signaling inhibits the development of mechanical allodynia and heat hyperalgesia in the carrageenan and CFA inflammatory pain models (Woolf et al. 1997; Tonussi and Ferreira 1999; Cunha et al. 2005; Inglis et al. 2005). Immediately after intraplantar injection of carrageenan or complete Freund's adjuvant (CFA) the hindpaw TNF levels begin rapidly increasing and this up-regulation persists in the inflamed paw for at least 5 days (Woolf et al. 1997; Cunha et al. 2005). There is also increased expression of TNFR1 and TNFR2 receptors within DRG tissues from inflammatory animal models (Li et al. 2004; Inglis et al. 2005). The TNFR1 is expressed exclusively on neuronal cells and the TNFR2 receptor is expressed exclusively on macrophages and/or monocytes in the DRG under inflammatory conditions (Li et al. 2004; Inglis et al. 2005). It has not been established which TNF receptor subtype contributes to inflammatory hyperalgesia, but it has been shown that the TNFR1 contributes to the development of mechanical and heat hyperalgesia after experimental nerve injury (Sommer et al. 1998). Collectively these data suggest that enhanced TNF signaling contributes to the development of inflammatory pain and we postulate that a similar mechanism could mediate the mechanical allodynia, hindpaw unweighting, and spinal Fos activation observed in the fracture model of CRPS.

The primary aim of this study was to determine whether blocking TNF signaling would prevent the development of the nociceptive, vascular, bone sequelae of fracture. Development of mechanical allodynia after fracture was blocked with sTNF-R1 treatment, whereas the development of hindlimb unweighting was only partially inhibited with sTNF-R1 treatment (Fig. 3). Fracture induced Fos expression in the lumbar dorsal horn was completely also blocked by sTNF-R1 treatment (Fig. 4, Fig. 5). Correlation analysis demonstrated a strong association between mechanical allodynia and ipsilateral Fos expression across all the dorsal horn laminae (Fig. 6). The labeling pattern observed in the present study resembles that reported after CFA-induced chronic inflammation (Abbadie and Besson 1992;Leah et al. 1996) and sciatic nerve chronic constriction injury (Kajander et al. 1996;Catheline et al. 1999;Yamazaki et al. 2001). The concentration of Fos labeling after the fracture was highest in laminae I–II which is heavily innervated by Aδ and C primary afferents, and it has been suggested that expression of Fos in these superficial laminae is a feature of cells involved in the processing of high threshold nociceptive input (Hunt et al. 1987;Menetrey et al. 1989). Furthermore, there was increased Fos labeling in deeper dorsal horn laminae III–IV and V–VI ipsilaterally and to a less extent V–VI contralaterally. Laminae III–IV receive mainly Aδ fiber connections from low-threshold mechanoreceptors (LaMotte 1977;Woolf and Fitzgerald 1986;Woolf 1987), while deep tissue nociceptive primary afferents Aδ and C terminate in laminae V–VI (Woolf and Fitzgerald 1986;Mense and Craig 1988;Hu and Zhao 2001). The increase in contralateral Fos expression observed after fracture is consistent with the studies using unilateral noxious stimuli and demonstrating increased Fos expression in the corresponding laminae on the opposite side of the spinal cord (Hunt et al. 1987;Menetrey et al. 1989;Yamazaki et al. 2001).

Surprisingly, post-fracture hindpaw edema and warmth was not inhibited by sTNF-R1 treatment (Fig. 3). These results indicate that TNF signaling is not required for the development of vascular abnormalities after fracture. Another component of CRPS is a regional loss of periarticular bone density (Bickerstaff et al. 1993;Sarangi et al. 1993). After distal tibia fracture there was a 32% loss of trabecular bone in the ipsilateral distal femur, a 19% loss in the L_4 vertebra, and a 13% nonsignficant reduction in the contralateral distal femur (Fig. 8 and Table 1). Also, trabecular thickness and connectivity declined after fracture and SMI increased in the ipsilateral distal femur, indicating a transformation to a more rod-like conformation (Table 1). The loss of trabecular connectivity and the shift to a more rod-like trabecular structure indicates that fracture induced trabecular resorption and perforation. No post-fracture cortical bone loss was observed in the midfemur. These findings are consistent with our previous experiments demonstrating a reduction in bone mineral density (BMD) in the distal femur and proximal tibia after unilateral sciatic nerve section or tibia fracture in rats, with no BMD changes observed in the diaphyses (Kingery et al. 2003a;Kingery et al. 2003b;Guo et al. 2004).

Multiple studies have showed that TNF is important in the pathogenesis of various forms of bone loss, such as rheumatoid arthritis, and can stimulate osteoclast formation and maturation (for review see (Boyce et al. 2005)). In the current study there was no significant difference in bone microarchitectural parameters between the sTNF-R1 and saline treatment cohorts at 4 weeks after fracture (Table 1). The lack of sTNF-R1 effect in the ipsilateral hindlimb indicates that TNF signaling does not play a role in the regional trabecular bone loss observed after fracture. The lack effect in the contralateral hindlimb is consistent with previously published studies demonstrating normal bone histomorphometry and BMD in TNF, TNFR1, and TNFR2 knockout mice, and in mice chronically treated with TNF antagonists (Kitazawa et al. 1994; Kimble et al. 1995; Roggia et al. 2001; Nanes 2003; Roggia et al. 2004).

In summary, the rat tibia fracture model was used to investigate the molecular mechanisms mediating the chronic inflammatory changes observed in CRPS. Increases in TNF expression were observed in skin, nerve and bone, and pre-emptive sTNF-R1 treatment inhibited the development of pain behavior and spinal Fos activation after fracture. It is unlikely that

systemically administered sTNF-R1 can penetrate the blood-brain barrier due to its high molecular weight (11,660 Da) and we postulate that the antinociceptive effects of sTNF-R1 were mediated in the skin and/or nerve tissues of the injured limb where increases in TNF expression were observed. These experimental data support the hypothesis that facilitated TNF signaling in injured tissues is an important mediator of chronic pain after fracture.

Acknowledgments

This study was supported by National Institutes of Health Grants GM65345 and DK67197. We would also like to thank Amgen for generously providing sTNF-R1.

References

Abbadie C, Besson JM. c-fos expression in rat lumbar spinal cord during the development of adjuvant-induced arthritis. Neuroscience 1992;48(4):985–993. [PubMed: 1630632]

Atkins RM, Duckworth T, Kanis JA. Features of algodystrophy after colles' fracture. J Bone Joint Surg 1990;72 B:105–110.

Bendele AM, McComb J, Gould T, Frazier J, Chlipala E, Seely J, Kieft G, Edwards CK 3rd. Effects of PEGylated soluble tumor necrosis factor receptor type I (PEG sTNF-RI) alone and in combination with methotrexate in adjuvant arthritic rats. Clin Exp Rheumatol 1999a;17(5):553–560. [PubMed: 10544838]

Bendele AM, McComb J, Gould T, Frazier J, Chlipala ES, Seely J, Kieft G, Wolf J, Edwards CK 3rd. Combination benefit of PEGylated soluble tumor necrosis factor receptor type I (PEG sTNF-RI) and dexamethasone or indomethacin in adjuvant arthritic rats. Inflamm Res 1999b;48(8):453–460. [PubMed: 10493163]

Benoliel R, Eliav E, Mannes AJ, Caudle RM, Leeman S, Iadarola MJ. Actions of intrathecal diphtheria toxin-substance P fusion protein on models of persistent pain. Pain 1999;79:243–253. [PubMed: 10068170]

Bickerstaff DR, Charlesworth D, Kanis JA. Changes in cortical and trabecular bone in algodystrophy. Br J Rheumatol 1993;32(1):46–51. [PubMed: 8422559]

Birklein F, Riedl B, Claus D, Neundorfer B. Pattern of autonomic dysfunction in time course of complex regional pain syndrome. Clin Auton Res 1998;8:79–85. [PubMed: 9613797]

Blumberg, H.; Janig, W. Clinical manifestations of reflex sympathetic dystrophy and sympathetically maintained pain. In: Wall, PD.; Melzack, R., editors. Book Title|, Vol. Volume|. City|: Publisher|, Year|. p.^pp. Pages|.

Bowden JJ, Garland AM, Baluk P, Lefevre P, Grady EF, Vigna SR, Bunnett NW, McDonald DM. Direct observation of substance P-induced internalization of neurokinin 1 (NK1) receptors at sites of inflammation. Proc Natl Acad Sci USA 1994;91:8964–8968. [PubMed: 7522326]

Boyce BF, Li P, Yao Z, Zhang Q, Badell IR, Schwarz EM, O'Keefe RJ, Xing L. TNF-alpha and pathologic bone resorption. Keio J Med 2005;54(3):127–131. [PubMed: 16237274]

Catheline G, Le Guen S, Honore P, Besson JM. Are there long-term changes in the basal or evoked Fos expression in the dorsal horn of the spinal cord of the mononeuropathic rat? Pain 1999;80(1–2):347–357. [PubMed: 10204748]

Cunha FQ, Poole S, Lorenzetti BB, Ferreira SH. The pivotal role of tumour necrosis factor alpha in the development of inflammatory hyperalgesia. Br J Pharmacol 1992;107(3):660–664. [PubMed: 1472964]

Cunha TM, Verri WA Jr, Silva JS, Poole S, Cunha FQ, Ferreira SH. A cascade of cytokines mediates mechanical inflammatory hypernociception in mice. Proc Natl Acad Sci U S A 2005;102(5):1755–1760. [PubMed: 15665080]

Delgado AV, McManus AT, Chambers JP. Production of tumor necrosis factor-alpha, interleukin 1-beta, interleukin 2, and interleukin 6 by rat leukocyte subpopulations after exposure to substance P. Neuropeptides 2003;37(6):355–361. [PubMed: 14698678]

Dickerson C, Undem B, Bullock B, Winchurch RA. Neuropeptide regulation of proinflammatory cytokine responses. J Leukoc Biol 1998;63(5):602–605. [PubMed: 9581804]

Edwards CKI, Frazier J, Seely J, Gaylord H, Martin S, Amiconne A, et al. Assessment of the major antigeniic epitopes of the recombinant human soluble p55 TNF Type I receptor: design of a novel monomeric non-immunogenic analog, sTNF-RI. Arthritis Rheum 1998;41:S58.

Empl M, Renaud S, Erne B, Fuhr P, Straube A, Schaeren-Wiemers N, Steck AJ. TNF-alpha expression in painful and nonpainful neuropathies. Neurology 2001;56(10):1371–1377. [PubMed: 11376190]

Feige U, Hu YL, Gasser J, Campagnuolo G, Munyakazi L, Bolon B. Anti-interleukin-1 and anti-tumor necrosis factor-alpha synergistically inhibit adjuvant arthritis in Lewis rats. Cell Mol Life Sci 2000;57 (10):1457–1470. [PubMed: 11078023]

Feldmann M. Development of anti-TNF therapy for rheumatoid arthritis. Nat Rev Immunol 2002;2(5): 364–371. [PubMed: 12033742]

Grell M, Wajant H, Zimmermann G, Scheurich P. The type 1 receptor (CD120a) is the high-affinity receptor for soluble tumor necrosis factor. Proc Natl Acad Sci U S A 1998;95(2):570–575. [PubMed: 9435233]

Guo TZ, Offley SC, Boyd EA, Jacobs CR, Kingery WS. Substance P signaling contributes to the vascular and nociceptive abnormalities observed in a tibial fracture rat model of complex regional pain syndrome type I. Pain 2004;108(1–2):95–107. [PubMed: 15109512]

Guo TZ, Wei T, Kingery WS. Glucocorticoid inhibition of vascular abnormalities in a tibia fracture rat model of complex regional pain syndrome type I. Pain 2006;121(1–2):158–167. [PubMed: 16472917]

Hildebrand T, Laib A, Muller R, Dequeker J, Ruegsegger P. Direct three-dimensional morphometric analysis of human cancellous bone: microstructural data from spine, femur, iliac crest, and calcaneus. J Bone Miner Res 1999;14(7):1167–1174. [PubMed: 10404017]

Hildebrand T, Ruegsegger P. A new method for the model-independent assessment of thickness in three-dimensional images. J Microsc 1997a;185:67–75.

Hildebrand T, Ruegsegger P. Quantification of Bone Microarchitecture with the Structure Model Index. Comput Methods Biomech Biomed Engin 1997b;1(1):15–23. [PubMed: 11264794]

Hu JY, Zhao ZQ. Differential contributions of NMDA and non-NMDA receptors to spinal Fos expression evoked by superficial tissue and muscle inflammation in the rat. Neuroscience 2001;106(4):823–831. [PubMed: 11682167]

Hunt SP, Pini W, Evan G. Induction of c-fos-like protein in spinal cord neurons following sensory stimulation. Nature 1987;328:632–634. [PubMed: 3112583]

Huygen FJ, De Bruijn AG, De Bruin MT, Groeneweg JG, Klein J, Zijistra FJ. Evidence for local inflammation in complex regional pain syndrome type 1. Mediators Inflamm 2002;11(1):47–51. [PubMed: 11930962]

Huygen FJ, Niehof S, Zijlstra FJ, van Hagen PM, van Daele PL. Successful treatment of CRPS 1 with anti-TNF. J Pain Symptom Manage 2004a;27(2):101–103. [PubMed: 15157033]

Huygen FJ, Ramdhani N, van Toorenenbergen A, Klein J, Zijlstra FJ. Mast cells are involved in inflammatory reactions during Complex Regional Pain Syndrome type 1. Immunol Lett 2004b;91 (2–3):147–154. [PubMed: 15019283]

Inglis JJ, Nissim A, Lees DM, Hunt SP, Chernajovsky Y, Kidd BL. The differential contribution of tumour necrosis factor to thermal and mechanical hyperalgesia during chronic inflammation. Arthritis Res Ther 2005;7(4):R807–R816. [PubMed: 15987482]

Jin X, Gereau RWt. Acute p38-mediated modulation of tetrodotoxin-resistant sodium channels in mouse sensory neurons by tumor necrosis factor-alpha. J Neurosci 2006;26(1):246–255. [PubMed: 16399694]

Junger H, Sorkin LS. Nociceptive and inflammatory effects of subcutaneous TNFalpha. Pain 2000;85 (1–2):145–151. [PubMed: 10692613]

Kajander KC, Madsen AM, Iadarola MJ, Draisci G, Wakisaka S. Fos-like immunoreactivity increases in the lumbar spinal cord following a chronic constriction injury to the sciatic nerve of rat. Neurosci Lett 1996;206(1):9–12. [PubMed: 8848286]

Kimble RB, Matayoshi AB, Vannice JL, Kung VT, Williams C, Pacifici R. Simultaneous block of interleukin-1 and tumor necrosis factor is required to completely prevent bone loss in the early postovariectomy period. Endocrinology 1995;136(7):3054–3061. [PubMed: 7789332]

Kingery WS, Davies MF, Clark JD. A substance P receptor (NK1) antagonist can reverse vascular and nociceptive abnormalities in a rat model of complex regional pain syndrome type II. Pain 2003a;104 (1–2):75–84. [PubMed: 12855316]

Kingery WS, Offley SC, Guo TZ, Davies MF, Clark JD, Jacobs CR. A substance P receptor (NK1) antagonist enhances the widespread osteoporotic effects of sciatic nerve section. Bone 2003b;33(6): 927–936. [PubMed: 14678852]

Kitazawa R, Kimble RB, Vannice JL, Kung VT, Pacifici R. Interleukin-1 receptor antagonist and tumor necrosis factor binding protein decrease osteoclast formation and bone resorption in ovariectomized mice. J Clin Invest 1994;94(6):2397–2406. [PubMed: 7989596]

LaMotte C. Distribution of the tract of Lissauer and the dorsal root fibers in the primate spinal cord. J Comp Neurol 1977;172(3):529–561. [PubMed: 402397]

Leah JD, Porter J, de-Pommery J, Menetrey D, Weil-Fuguzza J. Effect of acute stimulation on Fos expression in spinal neurons in the presence of persisting C-fiber activity. Brain Res 1996;719(1–2): 104–111. [PubMed: 8782869]

Li Y, Ji A, Weihe E, Schafer MK. Cell-specific expression and lipopolysaccharide-induced regulation of tumor necrosis factor alpha (TNFalpha) and TNF receptors in rat dorsal root ganglion. J Neurosci 2004;24(43):9623–9631. [PubMed: 15509749]

Liang D, Li X, Lighthall G, Clark JD. Heme oxygenase type 2 modulates behavioral and molecular changes during chronic exposure to morphine. Neuroscience 2003;121(4):999–1005. [PubMed: 14580950]

Maihofner C, Handwerker HO, Neundorfer B, Birklein F. Mechanical hyperalgesia in complex regional pain syndrome: a role for TNF-alpha? Neurology 2005;65(2):311–313. [PubMed: 16043808]

Martin S, Frazier J, Seely J, Amiconne A, Consenza ME, Rosenberg JJ, et al. A genetically modified tumor necrosis factor receptor I (sTNF-RI) that does not elicit antibody response in primates. Arthritis Rheum 1998;41:S58.

Mashiba T, Burr DB, Turner CH, Sato M, Cain RL, Hock JM. Effects of human parathyroid hormone (1–34), LY333334, on bone mass, remodeling, and mechanical properties of cortical bone during the first remodeling cycle in rabbits. Bone 2001;28(5):538–547. [PubMed: 11344054]

McComb J, Gould T, Chlipala E, Sennelo G, Frazier J, Kieft G, Seely J, Edwards CK 3rd, Bendele A. Antiarthritic activity of soluble tumor necrosis factor receptor type I forms in adjuvant arthritis: correlation of plasma levels with efficacy. J Rheumatol 1999;26(6):1347–1351. [PubMed: 10381054]

McDonald DM. Neurogenic inflammation in the rat trachea. I. Changes in venules, leucocytes and epithelial cells. J Neurocytol 1988;17(5):583–603. [PubMed: 3210042]

Menetrey D, Gannon A, Levine JD, Basbaum AI. Expression of c-fos protein in interneurons and projection neurons of the rat spinal cord in response to noxious somatic, articular, and visceral stimulation. J Comp Neurol 1989;285(2):177–195. [PubMed: 2503547]

Mense S, Craig AD Jr. Spinal and supraspinal terminations of primary afferent fibers from the gastrocnemius-soleus muscle in the cat. Neuroscience 1988;26(3):1023–1035. [PubMed: 3200424]

Molander C, Grant G. Laminar distribution and somatotopic organization of primary afferent fibers from hindlimb nerves in the dorsal horn. A study by transganglionic transport of horseradish peroxidase in the rat. Neuroscience 1986;19(1):297–312. [PubMed: 3785668]

Munnikes RJ, Muis C, Boersma M, Heijmans-Antonissen C, Zijlstra FJ, Huygen FJ. Intermediate stage complex regional pain syndrome type 1 is unrelated to proinflammatory cytokines. Mediators Inflamm 2005;2005(6):366–372. [PubMed: 16489257]

Myers RR, Campana WM, Shubayev VI. The role of neuroinflammation in neuropathic pain: mechanisms and therapeutic targets. Drug Discov Today 2006;11(1–2):8–20. [PubMed: 16478686]

Nanes MS. Tumor necrosis factor-alpha: molecular and cellular mechanisms in skeletal pathology. Gene 2003;321:1–15. [PubMed: 14636987]

Nichols ML, Allen BJ, Rogers SD, Ghilardi JR, Honore P, Luger NM, Finke MP, Li J, Lappi DA, Simone DA, Mantyh PW. Transmission of chronic nociception by spinal neurons expressing the substance P receptor. Science 1999;286:1558–1561. [PubMed: 10567262]

Oyen WJ, Arntz IE, Claessens RM, Van der Meer JW, Corstens FH, Goris RJ. Reflex sympathetic dystrophy of the hand: an excessive inflammatory response? Pain 1993;55(2):151–157. [PubMed: 8309706]

Rexed B. The cytoarchitectonic organization of the spinal cord in the cat. J Comp Neurol 1952;96(3): 414–495. [PubMed: 14946260]

Roggia C, Gao Y, Cenci S, Weitzmann MN, Toraldo G, Isaia G, Pacifici R. Up-regulation of TNF-producing T cells in the bone marrow: a key mechanism by which estrogen deficiency induces bone loss in vivo. Proc Natl Acad Sci U S A 2001;98(24):13960–13965. [PubMed: 11717453]

Roggia C, Tamone C, Cenci S, Pacifici R, Isaia GC. Role of TNF-alpha producing T-cells in bone loss induced by estrogen deficiency. Minerva Med 2004;95(2):125–132. [PubMed: 15272247]

Saade NE, Massaad CA, Ochoa-Chaar CI, Jabbur SJ, Safieh-Garabedian B, Atweh SF. Upregulation of proinflammatory cytokines and nerve growth factor by intraplantar injection of capsaicin in rats. J Physiol 2002;545(Pt 1):241–253. [PubMed: 12433964]

Sarangi PP, Ward AJ, Smith EJ, Staddon GE, Atkins RM. Algodystrophy and osteoporosis after tibial fractures. J Bone Joint Surg Br 1993;75(3):450–452. [PubMed: 8496220]

Sawamura S, Kingery WS, Davies MF, Agashe GS, Clark JD, Kobilka BK, Hashimoto T, Maze M. Antinociceptive action of nitrous oxide is mediated by stimulation of noradrenergic neurons in the brainstem and activation of [alpha]2B adrenoceptors. J Neurosci 2000;20(24):9242–9251. [PubMed: 11125002]

Sommer C, Kress M. Recent findings on how proinflammatory cytokines cause pain: peripheral mechanisms in inflammatory and neuropathic hyperalgesia. Neurosci Lett 2004;361(1–3):184–187. [PubMed: 15135924]

Sommer C, Schmidt C, George A. Hyperalgesia in experimental neuropathy is dependent on the TNF receptor 1. Exp Neurol 1998;151(1):138–142. [PubMed: 9582261]

Tonussi CR, Ferreira SH. Tumour necrosis factor-alpha mediates carrageenin-induced knee-joint incapacitation and also triggers overt nociception in previously inflamed rat knee-joints. Pain 1999;82 (1):81–87. [PubMed: 10422663]

Veldman PHJM, Reynen HM, Arntz IE, Goris RJA. Signs and symptoms of reflex sympathetic dystrophy: prospective study of 829 patients. Lancet 1993;342:1012–1016. [PubMed: 8105263]

Vogel C, Stallforth S, Sommer C. Altered pain behavior and regeneration after nerve injury in TNF receptor deficient mice. J Peripher Nerv Syst 2006;11(4):294–303. [PubMed: 17117937]

Weinberg AD, Montler R. Modulation of TNF receptor family members to inhibit autoimmune disease. Curr Drug Targets Inflamm Allergy 2005;4(2):195–203. [PubMed: 15853742]

Woolf CJ. Central terminations of cutaneous mechanoreceptive afferents in the rat lumbar spinal cord. J Comp Neurol 1987;261(1):105–119. [PubMed: 3624538]

Woolf CJ, Allchorne A, Safieh-Garabedian B, Poole S. Cytokines, nerve growth factor and inflammatory hyperalgesia: the contribution of tumour necrosis factor alpha. Br J Pharmacol 1997;121(3):417–424. [PubMed: 9179382]

Woolf CJ, Fitzgerald M. Somatotopic organization of cutaneous afferent terminals and dorsal horn neuronal receptive fields in the superficial and deep laminae of the rat lumbar spinal cord. J Comp Neurol 1986;251(4):517–531. [PubMed: 3782502]

Yamazaki Y, Maeda T, Someya G, Wakisaka S. Temporal and spatial distribution of Fos protein in the lumbar spinal dorsal horn neurons in the rat with chronic constriction injury to the sciatic nerve. Brain Res 2001;914(1–2):106–114. [PubMed: 11578603]

Zimmermann M. Ethical guidelines for investigations of experimental pain in conscious animals. Pain 1983;16:109–110. [PubMed: 6877845]

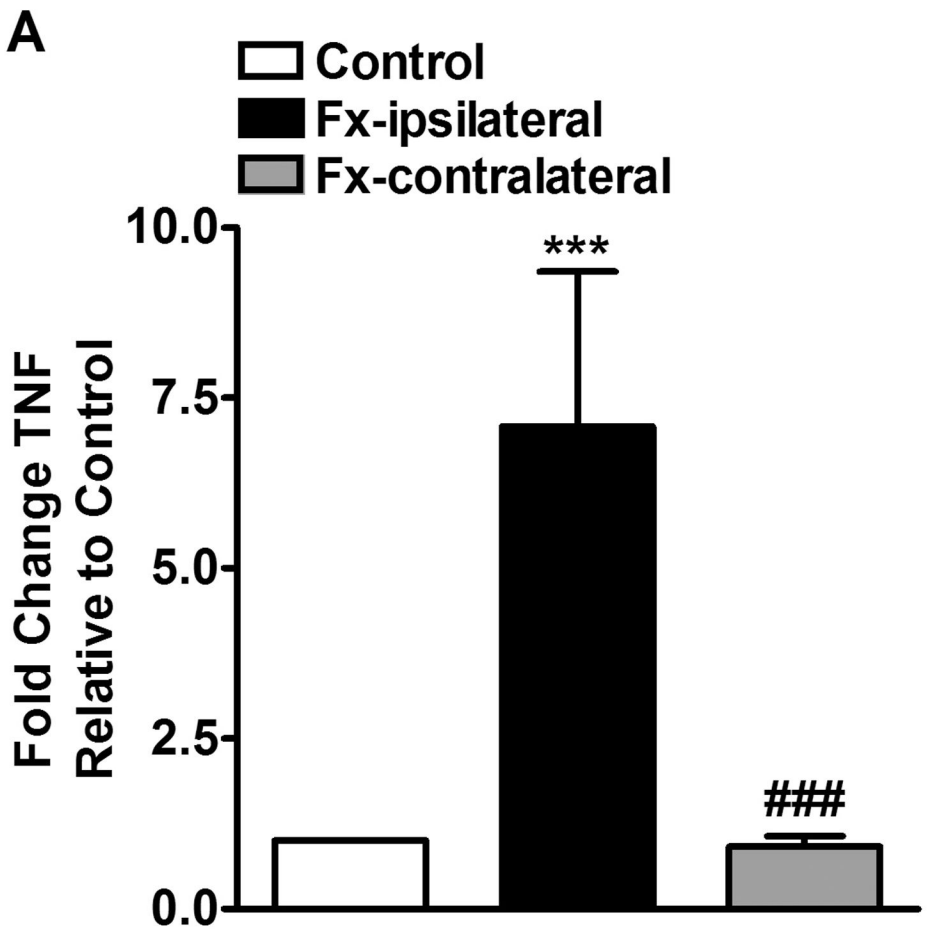

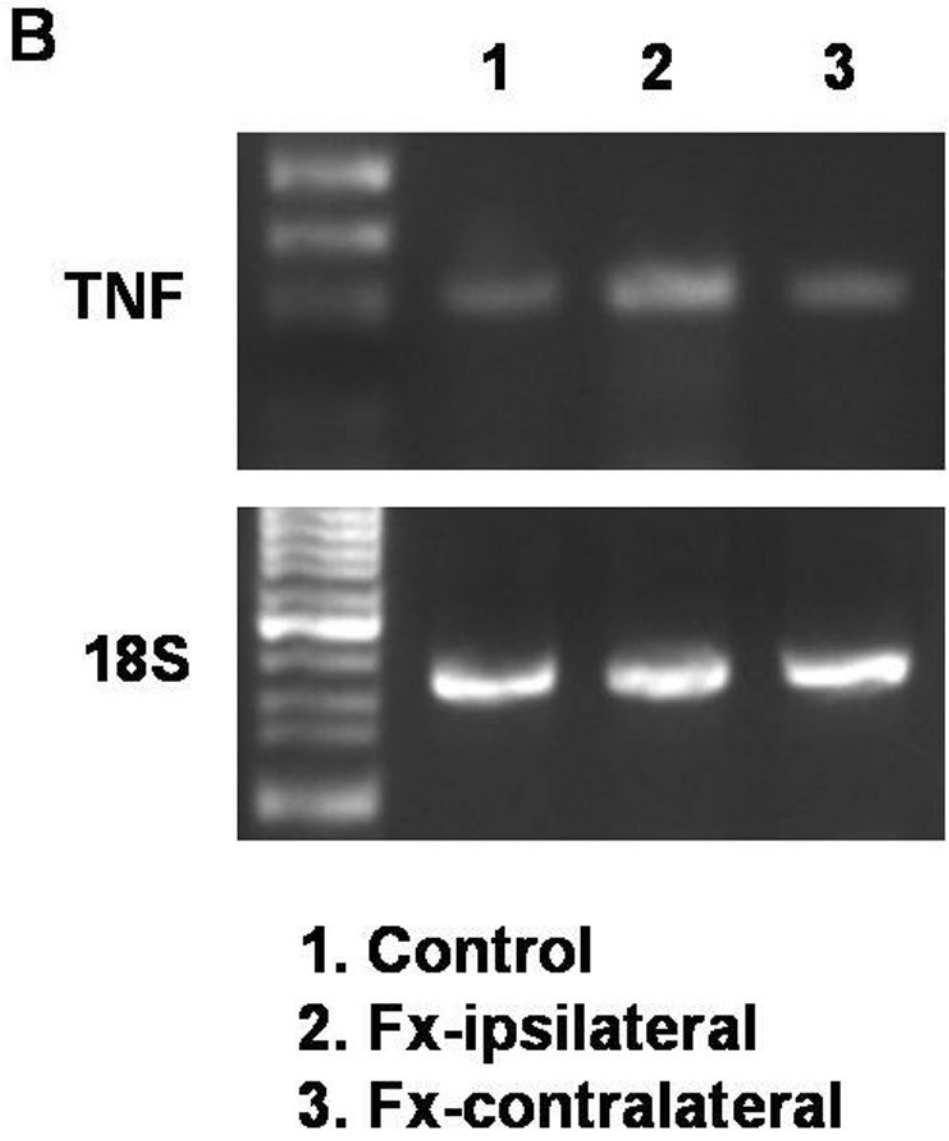

Figure 1.

Panel A shows PCR quantification of TNF mRNA levels in skin samples from hindpaws ipsilateral (Fx-ipsilateral) and contralateral (Fx-contralateral) to tibia fracture (n = 14), normalized to control samples (n = 10). At 4 weeks after fracture TNF expression was increased only in the ipsilateral hindpaw. Panel B shows the ethidium bromide bands derived from skin samples obtained from a control rat hindpaw and from the ipsilateral and contralateral hindpaws of a fracture rat.

*** $P < 0.001$

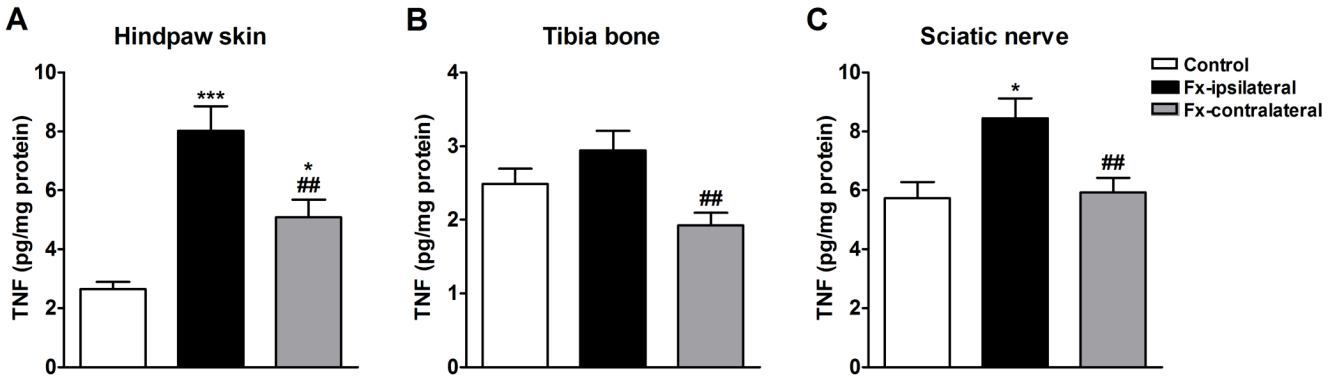

Figure 2.

TNF protein levels in rat hindpaw skin (A), tibia bone (B), and sciatic nerve (C) were determined by enzyme-linked immunoassay. Tissues were collected from the bilateral hindlimbs at 4 weeks after tibia fracture (n =14) or from control rats (n = 7). Fracture increased TNF protein levels in skin (A) and nerve(C), in the ipsilateral hindpaw relative to controls, and in skin, bone and sciatic nerve compared to the contralateral side.

*** $P < 0.001$ and * $P < 0.05$ for fracture *vs.* control values, $^{\#\#}$ $P < 0.01$ for ipsilateral *vs.* contralateral fracture values

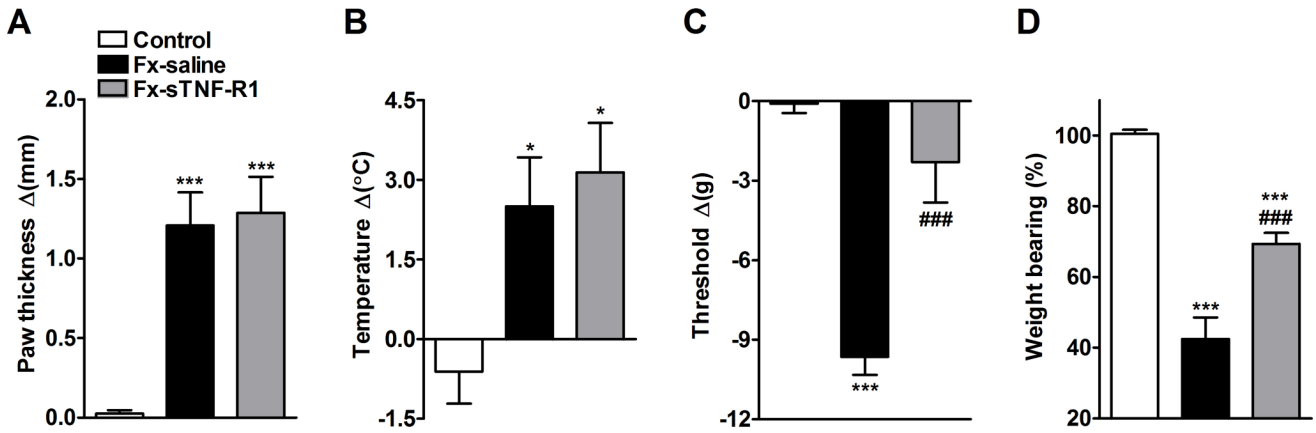

Figure 3.

After baseline testing, the right distal tibia was fractured and the hindlimb casted for 4 weeks. sTNF-R1 (n = 8, Fx-sTNF-R1) or saline (n = 7, Fx-saline) was subcutaneously injected every third day over a 4 week period after fracture. The sTNF-R1 treatment had no effect on the hindpaw edema (A) or warmth (B), but did reverse hindpaw mechanical allodynia (C) and the hindlimb unweighting (D) that developed after fracture. Measurements for (A), (B), and (C) represent the difference between the fracture side and the contralateral paw, thus a positive value represents an increase in thickness or temperature on the fracture side, a negative value represents a decrease in mechanical nociceptive thresholds on the affected side. Measurements for (D) represent weight bearing on the fracture hindlimb as a ratio to 50% of bilateral hindlimb loading, thus a percentage lower than 100% represents hindpaw unweighting.

* $P < 0.05$, *** $P < 0.001$ fracture *vs.* control values, and $^{\#\#\#}$ $P < 0.001$ fracture sTNF-R1 treatment *vs.* fracture saline treatment.

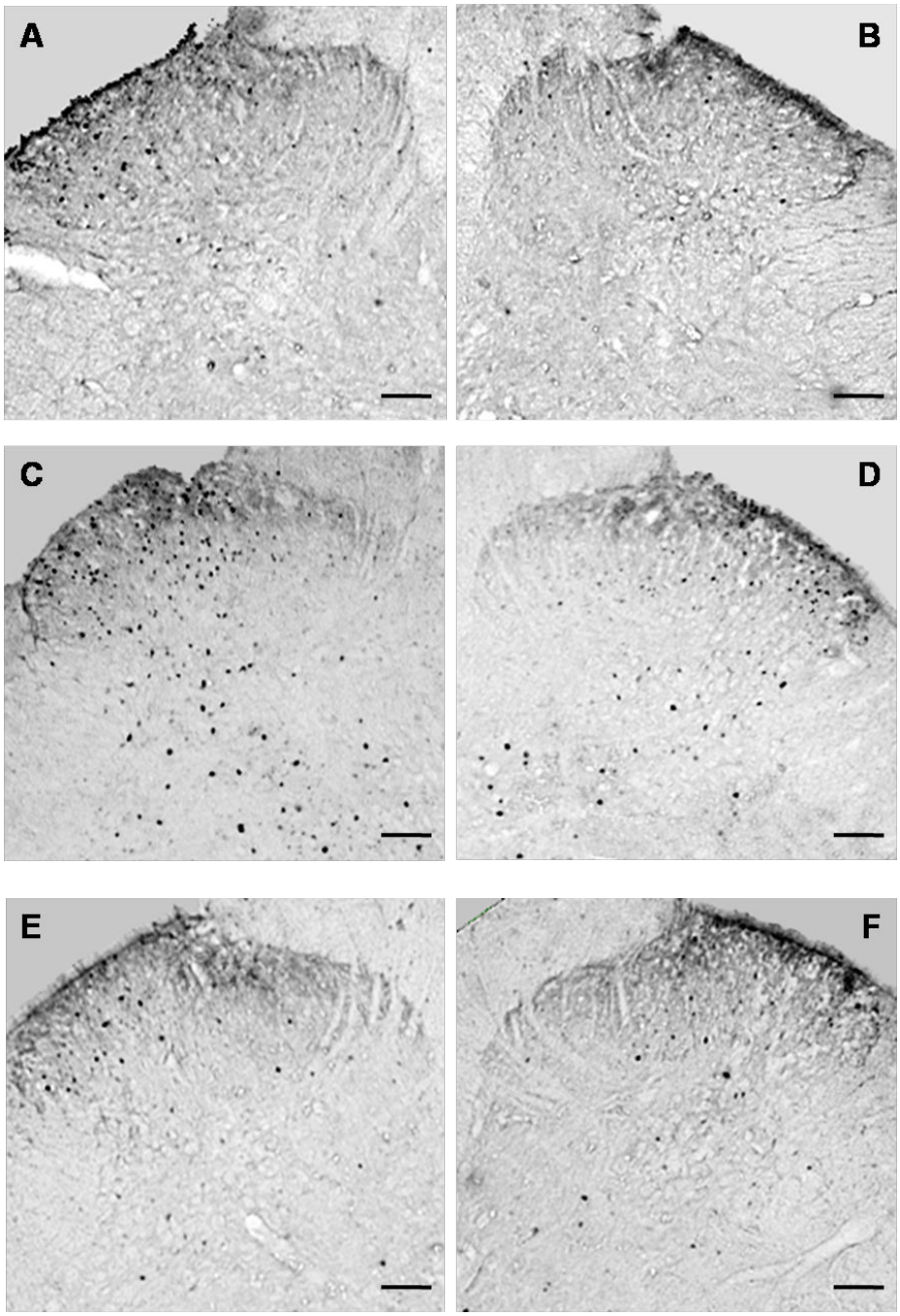

Figure 4.

Microphotographs illustrating the distribution of Fos-IR neurons in the lumbar (L4–L5 segments) spinal cord dorsal horn. All images of the spinal cord were captured with a 4X objective. Panels A and B demonstrate the right and left sides, respectively, of a control rat spinal cord section. Panels C and D demonstrate the ipsilateral and contralateral sides, respectively, of a tibia fracture rat treated with saline. A dense Fos immunostaining can be seen in the superficial laminae (I and II) and through the deep laminae in the ipsilateral (C) and in the contralateral dorsal horn (D). Treatment with sTNF-R1 blocked this increase in Fos-IR in the ipsilateral and contralateral dorsal horn of a tibia fracture rat (E and F respectively). The scale bar represents 100μm.

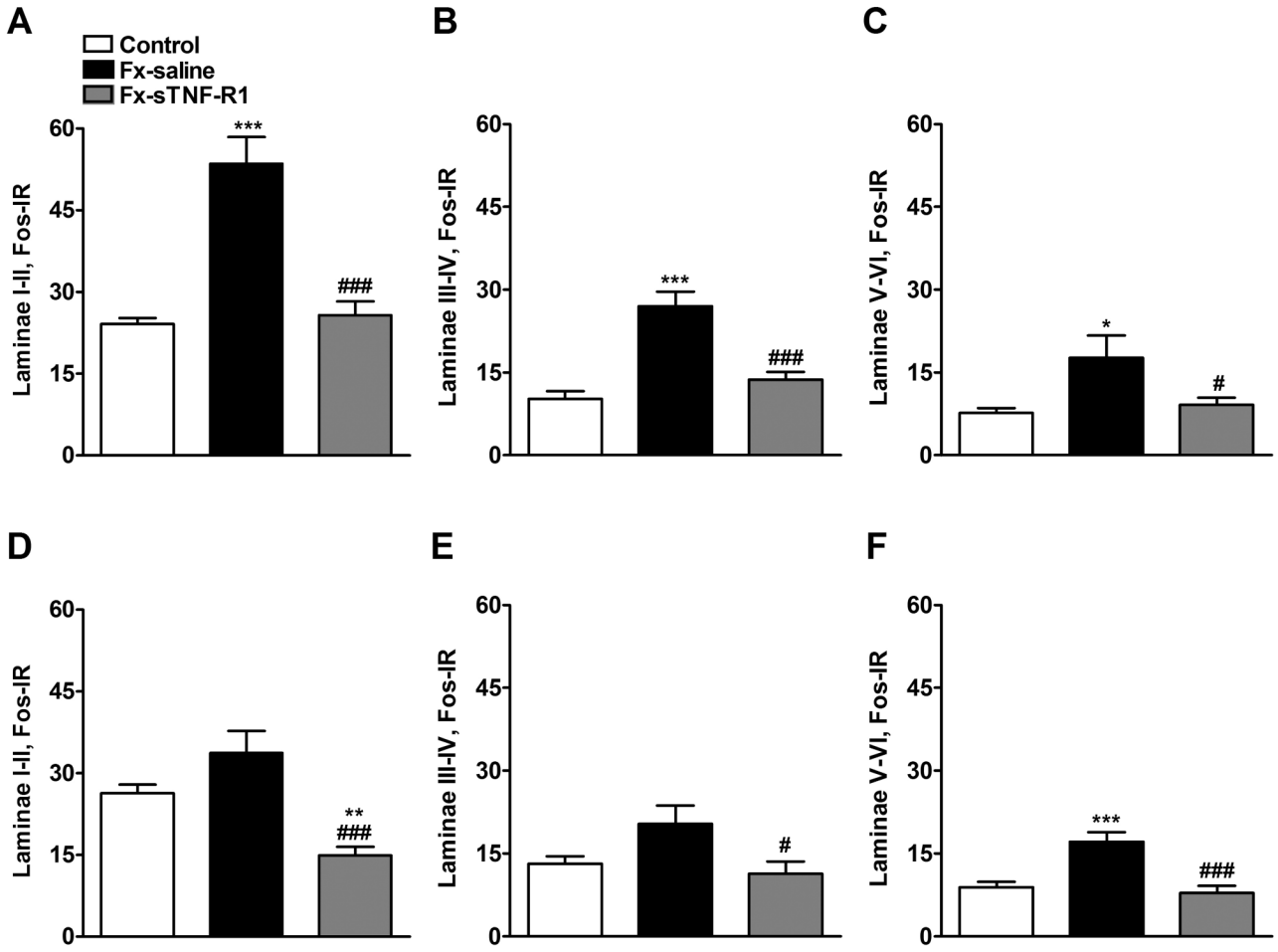

Figure 5.

Four weeks after tibia fracture and casting the L4, L5 lumbar spinal cord segments were sectioned and stained for Fos immunoreactivity. Results are expressed as the mean number of spinal Fos-IR neurons/section (± SEM), per dorsal horn laminar region (laminae I + II, III + IV and V + VI). Graphs (A), (B), and (C) represent the right side of the spinal cord (ipsilateral to the fracture side), whereas graphs (D), (E), and (F) represent the left side of the spinal cord (contralateral to the fracture side). Fracture (Fx) increased Fos expression in all three dorsal horn laminar regions ipsilateral to fracture, and in laminar region V+VI contralateral to fracture. Treatment with sTNF-R1 (n=9, Fx-sTNF-R1) significantly decreased fracture induced spinal Fos expression, compared to the saline treated tibia fracture rats (n=9, Fx-saline).

* $P < 0.05$, ** $P < 0.01$, *** $P < 0.001$ fracture saline treatment *vs.* control group (n=9), and $^{\#}$ $P < 0.05$, $^{\#\#\#}$ $P < 0.001$ fracture sTNF-R1 treatment *vs.* fracture saline treatment.

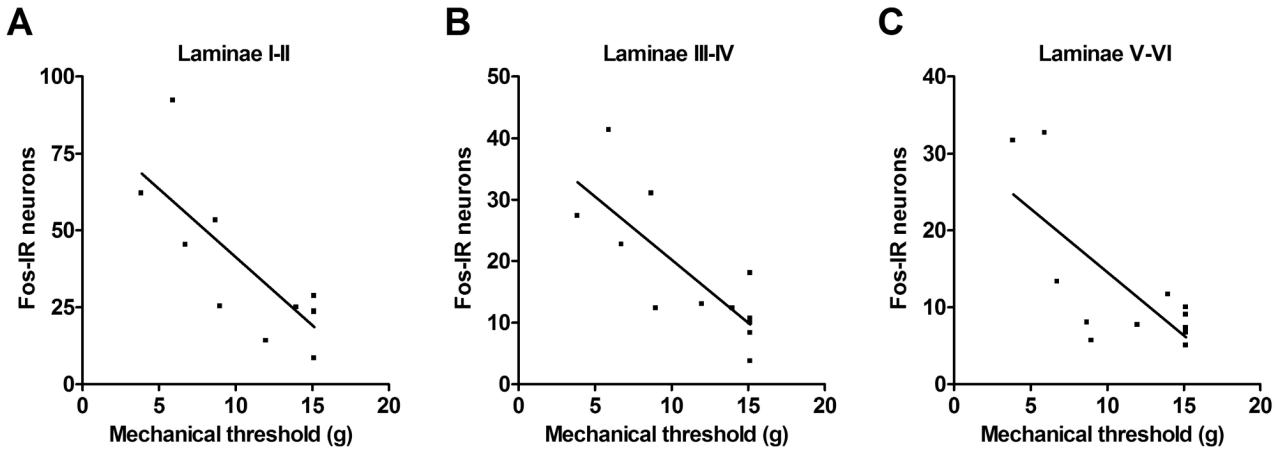

Figure 6.

Linear regression demonstrated a significant correlation between the extent of the mechanical allodynia in the fracture hindlimb and number of Fos positive spinal neurons in the ipsilateral laminae I–II (A, $P = 0.004$, $R^2 = 0.587$), laminae III–IV (B, $P = 0.003$, $R^2 = 0.597$), and laminae V–VI (C, $P = 0.006$, $R^2 = 0.548$).

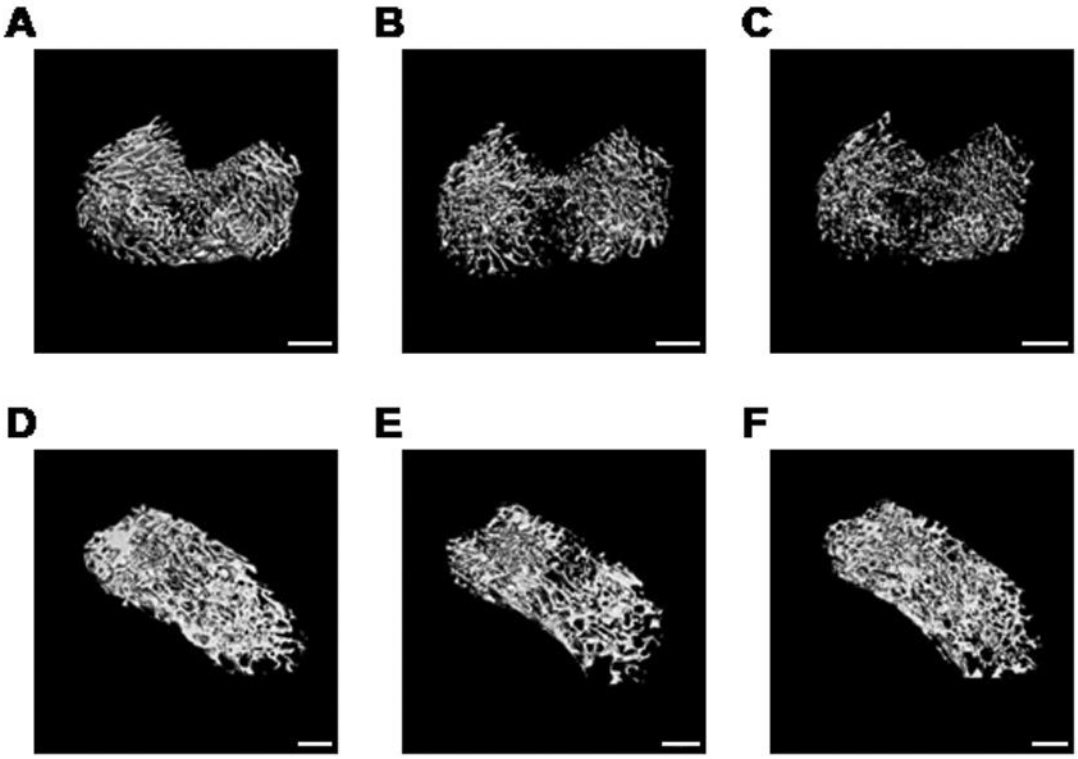

Figure 7.

Three dimensional microCT images of the ipsilateral distal femur (A, B, C) and L4 vertebra (D, E, F) illustrating changes in the trabecular bone compartment at 4 weeks after tibia fracture. Scans A and D are from a control rat; B and E are from a fracture rat treated with saline; and C and F are from a fracture rat treated with sTNF-R1. There was a marked regional loss of trabecular bone after tibia fracture (B, E), which was unaltered by preemptive sTNF-R1 treatment (C, F). White bar represents 1 mm.

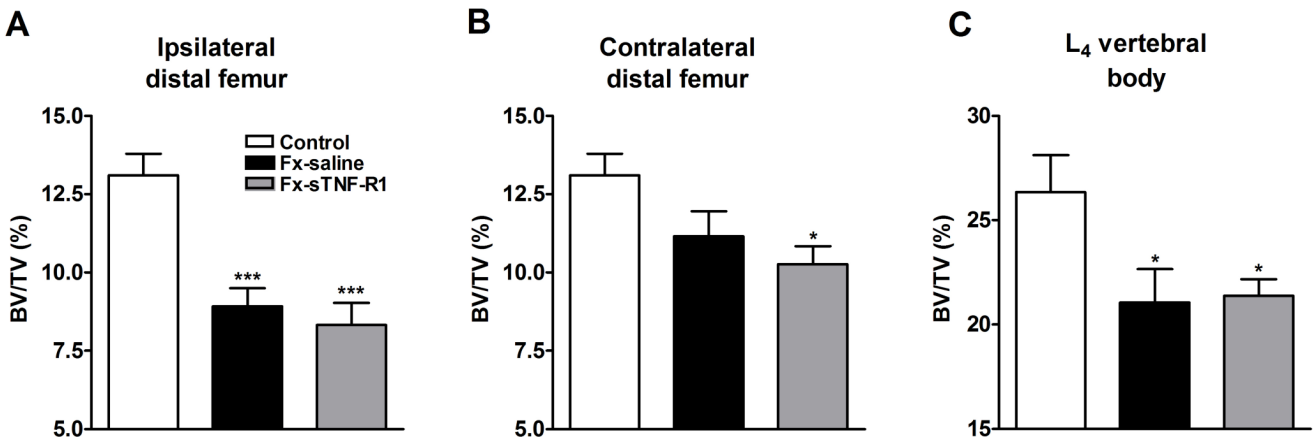

Figure 8.

After the right tibia was fractured and the hindlimb casted for 4 weeks the rats were sacrificed and the bilateral distal femurs and L_4 vertebrae were collected for *ex-vivo* μCT scanning. After tibia fracture with 4-weeks saline treatment (Fx-saline) there was extensive regional trabecular bone loss in the ipsilateral (A) and contralateral (B) distal femur, as well as in the L_4 vertebra (compaired to control rats, n = 11 per cohort for distal femur and n = 8 per cohort for vertebral data). There was no effect on midfemur cortical bone (data not shown). A 4-week course of sTNF-R1 treatment (FX-sTNF-R1) had no effect on the development of trabecular bone loss in any region of interest.

* $P < 0.05$, *** $P < 0.001$ *vs.* control group.

Table 1

Distal femur and L_4 vertebral trabecular bone evaluated by μCT

	n	BV/TV (%)	Tb.N (mm^{-1})	Tb.Th (μm)	Tb.Sp (μm)	Conn.D (mm^{-3})	SMI (0–3)
Ipsilateral DF							
Control	11	13.1 ± 0.7	2.6 ± 0.12	74.6 ± 1.7	393.0 ± 18.6	29.2 ± 2.4	2.0 ± 0.05
Fx-saline	11	**8.9 ± 0.6*****	2.4 ± 0.10	**67.7 ± 1.5****	432.2 ± 18.9	**18.3 ± 1.8*****	**2.5 ± 0.06*****
Fx-sTNF-R1	11	**8.3 ± 0.7*****	2.4 ± 0.08	**67.1 ± 1.5****	437.8 ± 14.9	**16.0 ± 2.1*****	**2.6 ± 0.11*****
Contralateral DF							
Control	11	13.1 ± 0.7	2.6 ± 0.12	74.6 ± 1.7	393.0 ± 18.6	29.2 ± 2.4	2.0 ± 0.05
Fx-saline	11	11.4 ± 0.8	2.5 ± 0.14	73.4 ± 2.1	413.5 ± 23.3	24.2 ± 2.3	**2.3 ± 0.05***
Fx-sTNF-R1	11	**10.3 ± 0.6***	2.5 ± 0.10	69.8 ± 1.1	418.9 ± 17.6	22.7 ± 1.8	**2.4 ± 0.07*****
L_4 vertebral body							
Control	8	25.3 ± 1.8	3.5 ± 0.17	86.5 ± 1.8	294.2 ± 15.2	59.7 ± 5.0	0.8 ± 0.17
Fx-saline	8	**20.6 ± 1.8***	3.5 ± 0.16	**78.8 ± 1.9****	291.5 ± 14.3	58.8 ± 6.2	**1.5 ± 0.15****
Fx-sTNF-R1	8	**21.4 ± 0.8***	3.6 ± 0.09	**81.1 ± 0.9***	278.6 ± 6.8	61.9 ± 3.4	**1.5 ± 0.07****

Structural changes measured *ex vivo* by μCT at 4 weeks after fracture. All data expressed as means ± SE.

* $p < 0.05$

** $p < 0.01$

*** $p < 0.001$ for fracture *vs* control values.